Proton Tunneling in the Loss of Hydrogen Bromide from Energy-Selected Gas-Phase 2-Bromobutane Cations

Jeffrey W. Keister and Tomas Baer*

Chemistry Department, University of North Carolina at Chapel Hill, Chapel Hill, North Carolina 27599-3290

Roland Thissen and Christian Alcaraz

Laboratoire pour l'Utilization de Rayonnement Electromagnetique, Bât. 209d, Université Paris-Sud, F-91405 Orsay Cedex, France

Odile Dutuit

Laboratoire de Physico-Chimie des Rayonnements, Bât. 350, Centre Universitaire d'Orsay, F-91405 Orsay Cedex, France

Henri Audier and Valerie Troude

École Polytechnique, Laboratoire des Mécanismes Réactionnels, F-91128 Palaiseau Cedex, France

Received: October 14, 1997; In Final Form: December 11, 1997

The dissociation dynamics of energy-selected 2-bromobutane ions has been investigated by photoelectron photoion coincidence (PEPICO). The data were collected with a conventional gas discharge light source at the University of North Carolina and at the SuperACO synchrotron storage ring of LURE in Orsay, France. The 2-bromobutane ion dissociates via Br and HBr loss within 0.3 eV of the ionization limit. The Br loss channel produces the *sec*-butyl ion $C_4H_9^+$ via a simple bond cleavage and is found to proceed at a fast rate. At lower ion energies, the HBr loss channel produces the 2-butene ion via a concerted mechanism with rate constants in the microsecond range. A model that involves tunneling associated with the proton transfer is proposed. Asymmetric time-of-flight distributions and breakdown diagrams are fitted to the statistical RRKM theory with the aid of GAUSSIAN ab initio molecular orbital calculations at the MP2/6-31G* level. The fitting of the data was optimized for a barrier height of 0.438 eV and an imaginary frequency associated with the H atom transfer step of 1245 cm^{-1}. This compares with the ab initio results of 0.796 eV and 1265 cm^{-1}. Heats of formation at 0 K for 2-bromobutane cation (880.1 ± 2.7 kJ mol^{-1}) and *sec*-butyl cation (794 ± 3 kJ mol^{-1}) were derived from this work.

Introduction

Tunneling is frequently invoked to explain kinetic results that are not consistent with RRKM or transition-state theory. This is especially the case when a reaction involves the motion of H atoms or protons. However, for a variety of reasons quantitative evidence for tunneling is often elusive. In thermal reaction systems with their attendant broad distribution of internal energies, the fraction of reaction events that proceed via tunneling is often masked by the much larger fraction of molecules that has sufficient energy to pass over the barrier at rates far in excess of the tunneling rates. Thus, only in energy-selected systems in which it is possible to excite a molecule to an energy region below such a barrier does the effect of tunneling become clearly evident. However, in neutral systems it is often difficult to prepare a molecule in a given energy level because of, among other things, poor Franck−Condon factors. Several clear cases of tunneling have been investigated in recent years.[1−6] One is the $H_2CO \rightarrow H_2 + CO$ reaction.[1,2] For experimental reasons, it was possible only to investigate the deuterated analogue of this reaction because at the accessible energy region, formaldehyde-h_2 dissociated more rapidly than could be measured. Another known reaction is the HCl loss from ethyl chloride ions. Here photoelectron photoion coincidence (PEPICO) methods were used to prepare C_2H_5Cl ions with energies well below the classical barrier for reaction.[3,4] As in the formaldehyde case, all reaction products were formed exclusively by tunneling. However, in the case of ethyl chloride, it was possible to compare the dissociation rates for $C_2H_5Cl^+$ and $C_2D_5Cl^+$. RRKM analysis in conjunction with ab initio molecular orbital calculations of vibrational frequencies was used to prove that this reaction proceeds via quantum-mechanical tunneling. Finally, a reaction that has some similarities to the one under investigation here is CH_3 and CH_4 loss from acetone ions.[5] Heinrich et al. modeled the slow loss of CH_4, which involves a hydrogen atom transfer, by a tunneling mechanism. Ab initio calculations of the transition-state vibrational frequencies, including the imaginary frequency associated with the reaction coordinate, were used to calculate the dissociation rates. Unfortunately, no energy-selected CH_4 loss measurements have been reported.

Ionic reactions would appear to offer an abundance of tunneling possibilities because a large fraction of ionic dissociations proceed via H or H^+ transfer prior to fragmentation. However, detailed ab initio calculations have shown that the transition state, or rate-limiting step, for such reactions may not involve the H or H^+ transfer.[7] In such cases, tunneling may

S1089-5639(97)03338-0 CCC: $15.00
Published on Web 01/22/1998

occur, but the H or D atom transfer will not be rate limiting, so the tunneling reaction remains hidden. If the rate-limiting step really does involve tunneling, then the isotope effect on the dissociation rate will be very large. Thus, the observation of very different dissociation rate constants for H and D atom transfer can be used to prove that the reaction is proceeding by tunneling. This proof is best accomplished by modeling the rate constants with a version of the statistical RRKM theory that includes the tunneling correction.[8,9] Small isotope effects on the dissociation rate[10] ($k_H/k_D \sim 1-10$) can usually be explained in terms of the vibrational zero-point energy effect on the activation energy and the effect of the lower C−D frequencies on the ion density of states.

The dissociative photoionization of 2-bromobutane has been previously studied.[11,12] This ion shares with ethyl chloride the distinction that HX loss is the observed lowest energy dissociation path. All other alkyl halide ions, from ethyl through butyl, dissociate via simple halide atom loss.[13−16] This is in spite of the fact that, in every case, the HX + $C_nH_{2n}^+$ energy is considerably less than the X + $C_nH_{2n+1}^+$ energy. Apparently, the barrier for H atom transfer to the halogen atom is higher than the threshold for halide atom production, which occurs in most cases with no reverse activation barrier.

Another feature that ethyl chloride and 2-bromobutane (as well as acetone) ions share is that the HX loss reaction is slow, leading to metastable or long-lived ions that decay on the microsecond time scale. This is in spite of the fact that the experimentally measured onset for dissociation is close to the ionization limit. If this measured onset can indeed by equated to the activation energy, E_0, then the rate as calculated by RRKM theory should be very fast, which conflicts with the low measured rate constants. This in itself is evidence for tunneling. That is, if the classical barrier were much higher than the measured onset, the reaction could occur only by tunneling through this barrier, thus slowing down the reaction rate. However, slow rate constants can also be caused by prior isomerization to a much more stable structure, followed by dissociation. This possibility may be ruled out if one can ascertain that there is effectively no competition between the direct (−X) and indirect (−HX) loss reactions.

We have thus undertaken this PEPICO study of the dissociation dynamics of 2-bromobutane ions in order to determine whether the slow rate constant associated with HBr loss is a result of tunneling through an H atom transfer barrier. The experimental results are analyzed with tunneling-corrected RRKM statistical theory using vibrational frequencies obtained from ab initio molecular orbital calculations.

Experimental Approaches

In this work, two apparatuses were used. At UNC, a continuous hydrogen discharge lamp with a 1 m monochromator is used to provide tunable VUV photon energies in the 8−12 eV range.[17,18] Threshold electrons are selected using a combination steradiancy analyzer and hemispherical electrostatic energy analyzer (ESA) to give a total electron energy resolution of ∼45 meV. The resolution is provided by the 10 cm long electron drift region (steradiancy analyzer) which has a high collection efficiency for threshold electrons and discriminates against energetic electrons with off-axis velocity components. However, energetic (hot) electrons ejected along the electron TOF axis are not stopped by either the drift tube or the ESA, whose resolution of 2 eV does not influence the total resolution of the apparatus. The main disadvantage of this energy analysis, compared to the LURE approach which we describe shortly, is that the electron signal is always contaminated by a small fraction of hot electrons.

The ions and electrons were accelerated out of the ionization region with a continuous electric field of 20 V/cm. Coincident ion TOF spectra were accumulated by using a time-to-pulse height converter and multichannel analyzer which measures the distribution of time differences between electron and ion detector pulses. The ions are accelerated to 100 eV in the first 5 cm long acceleration region. A short space-focusing second region accelerates the ions to 220 eV, after which they drift for 30 cm and are detected by a multichannel plate detector. Slowly dissociating ions, so-called metastable ions, fragment in the first acceleration region. The resulting daughter ion TOF distribution is asymmetrically broadened toward long TOF. The 2-bromobutane ions require 8.39 μs to reach the end of the first acceleration region. Thus, dissociation events occurring after that time resulted in a flight time indistinguishable from that of the parent ions. That is, daughter ions formed in the drift region were collected as parent ions.

Both thermal and molecular beam samples were used at UNC. The total backing pressure of the molecular beam source was 240 Torr, of which 25% was bromobutane sample and 75% was Ar. The beam was formed using a 50 μm nozzle and 1 mm skimmer. The internal temperature of the gas produced by the nozzle expansion was 230 K (ca. 80 meV average internal energy of the bromobutane gas). An important advantage of using this sample source was the increased mass resolution due to the low transverse translational energy of the skimmed beam. This permitted mass peaks due to HBr and Br loss channels to be readily resolved.

At LURE, the light source is the SuperACO electron storage ring, which is operated in two-bunch mode to allow TOF energy analysis of electrons.[19,20] The SAPHIRS (Spectroscopie d'Agregats PHotoIonises par Rayonnement Synchrotron) experimental setup was used (see ref 20 for details). Briefly, a 3 m monochromator is used to disperse the broad-band radiation from a bending magnet in the ring. To provide ∼13 meV electron energy resolution, a 1 V/cm field is used to extract the electrons. The time between photon pulses from the storage ring of 120 ns is sufficient to permit time-of-flight analysis of the electrons with a 4 cm long drift region and thus to distinguish the threshold electrons from energetic electrons whose initial ejection angle is directed at the electron detector. Once a threshold electron is counted, a 60 V/cm field is pulsed on to extract the coincident ion. The acceleration distance for ions is now only 0.75 cm, so that the bromobutane parent ions are accelerated for only 1.88 μs in this first region. However, the total delay prior to the extraction pulse, which is determined by the electron TOF ($\tau_e = 0.05$ μs) and the inherent delay in the application of the ion extraction pulse ($\tau_d = 0.20$ μs), is 0.250 μs. Thus, the parent ions spend 2.13 μs in the first acceleration region. The advantage of this pulsing arrangement is that the electron resolution is very high because of the low electric field and the TOF analysis. The disadvantage for measuring dissociation rate constants of metastable ions is that the first 0.25 μs is lost and that the shape of the fragment ion signal from slowly dissociating ions is a combination of a sharp peak, which originates from the fragment ions produced during the 0.25 μs delay and the asymmetric peak due to dissociation during the 1.88 μs in the first acceleration region. The total drift distance for the ions was 15 cm.

At LURE, a room-temperature 50 μm nozzle pressurized to 60 Torr (the vapor pressure of bromobutane) was used to expand a neat sample beam through a skimmer. Although this provided

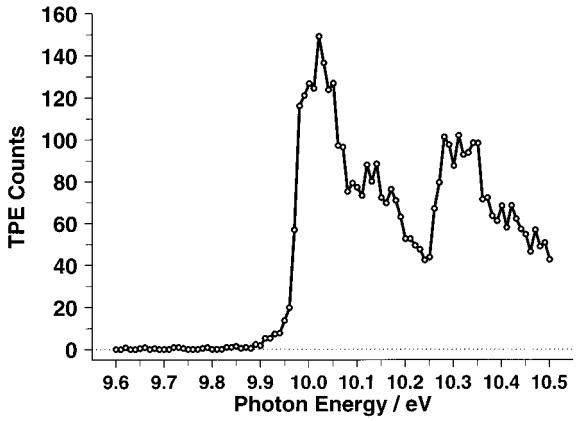

Figure 1. Threshold photoelectron spectrum of 2-bromobutane, obtained at LURE. The adiabatic and vertical ionization energies were found to be 9.98 and 10.02 eV, respectively. The signal near 10.3 eV is due to the higher energy spin−orbit peak. Each point corresponds to 1 s accumulation time.

no cooling of the internal degrees of freedom, it significantly improved the mass resolution because the skimmed beam had a very low transverse translational temperature. The use of a seeded beam with up to 1000 Torr of argon in this apparatus provided better cooling of the internal modes but also produced many clusters. Potential complications due to clusters was thus avoided by the use of a thermal beam. The only disadvantage of this setup is the broad internal energy distribution with its average rotational and vibrational energy of 138 meV.

Results

A threshold photoelectron spectrum (TPES) of 2-bromobutane obtained at LURE is shown in Figure 1. The two dominant peaks are due to the two spin−orbit states associated with the bromine atom.[21] We can use this spectrum to assign a value for the adiabatic IE of 9.98 ± 0.02 eV and a vertical (maximum TPES signal) IE of 10.02 ± 0.03 eV. With the neutral heat of formation from Pedley et al.,[22] this gives a 0 K ion heat of formation of 880.1 ± 2.7 kJ mol^{-1}. The conversion from room temperature to 0 K is accomplished with the use of the integrated elemental heat capacities from the JANAF tables[23] and the molecular heat capacity that is obtained using our ab initio MO calculations of the neutral and ion vibrational frequencies as discussed in the next section.

Sample TOF spectra are shown in Figures 2 and 3. The continuous ion extraction in the UNC apparatus (Figure 2) shows a sharp peak due to Br loss and production of the mass 57 $C_4H_9^+$ ion. This sharp and symmetric peak indicates that this dissociation is rapid on the time scale of the experiment, i.e., $k > 10^7$ s^{-1}. On the other hand, the metastable HBr loss daughter ion, $C_4H_8^+$ with mass 56, has a peak that is asymmetrically broadened to longer flight times because the reaction is taking place while the ion is being accelerated in the 5 cm long acceleration region. Rate constants can be obtained by fitting the asymmetric mass 56 fragment ion peak. Because the HBr loss reaction rate constant increases rapidly as a function of energy, any single rate constant associated with this broad 220 K distribution of bromobutane ions ($\langle E \rangle = 80$ meV) is in general not the same as the 0 K rate constant. The solid line through the data points thus corresponds to a calculated TOF distribution with an "effective" rate constant obtained by accounting for the thermal energy distribution. This method has recently been applied to the dissociation of butadiene at 298 and 220 K.[24]

The LURE data in Figure 3 are a composite of three TOF distributions obtained by varying the delay in extracting the ions

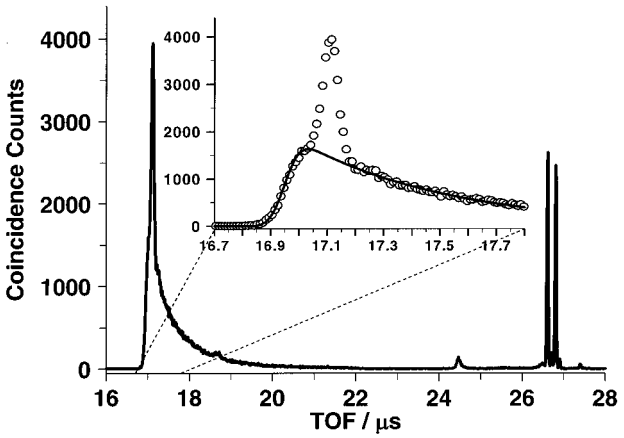

Figure 2. Sample TOF data obtained at UNC. The two strong parent ion peaks near 26.7 μs show the two Br isotopes. Small peaks at 18.7 and 24.4 μs are due to a background of other compounds which were run previously. At 10.2 eV, we see considerable metastable signal due to HBr loss. The inset shows a blowup of the region where the metastable mass 56 and the fast mass 57 peaks can be distinguished from each other. The solid line through the experimental data points in the inset is a result of modeling the metastable mass 56 ion TOF distribution using the derived rate constant function in Figure 9. This spectrum was acquired in roughly 16 h.

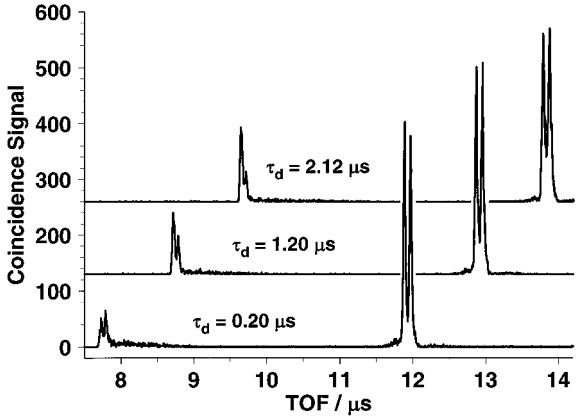

Figure 3. TOF data obtained with the synchrotron at LURE. The spectra were collected at 10.00 eV photon energy with different pulser delays. The total signal of each spectrum has been adjusted to be the same for all three in order to show that increasing the delay time increases the mass 56 peak intensity but not the mass 57 peak intensity. The signal just to the left of the parent ion peaks is due to metastable dissociation products formed in the drift tube and accelerated ahead of parent ions near the ion detector. As the delay time is increased, the sharp mass 56 TOF peak intensity (associated with loss of HBr which occurs before the application of the ion extraction pulse) increases at the expense of parent ion and metastable signals. Each spectrum was accumulated in about 20 min and consists of about 9800 coincidence counts.

out of the acceleration region. As in the UNC data, the $C_4H_9^+$ (m/z 57) peak is symmetric because it is the result of a fast dissociation. However, the $C_4H_8^+$ peak also has a sharp part (the first peak) due to dissociation prior to application of the acceleration pulse and an asymmetric part due to dissociation while the ion was accelerated for 1.88 μs. The sharp component remains nearly symmetric because the ions do not move a significant distance in the 1 V/cm electric field prior to the application of the 60 V/cm field. By increasing the delay time, the fraction of ions that dissociate before pulse extraction is increased so that the sharp component of the metastable peak increases with delay time. Although the m/z 57 peak remains constant with increasing τ_d, the m/z 56 peak increases because

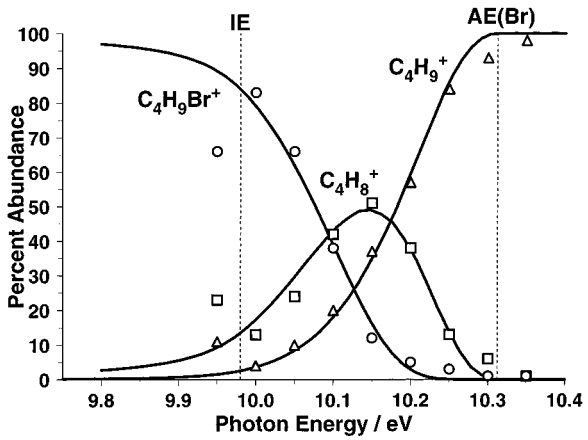

Figure 4. Full breakdown diagram showing the fractional abundance of the parent ion, $C_4H_9^+$, and $C_4H_8^+$ ions as a function of the photon energy. The solid line is a calculated breakdown diagram using the tunneling rate constants shown in Figure 9.

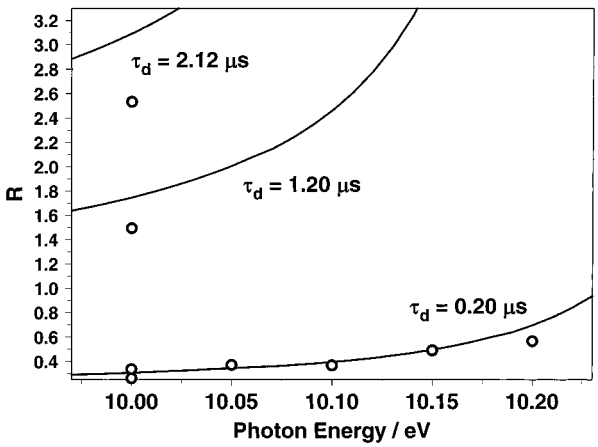

Figure 5. Ratio R of sharp (symmetric) to broad (asymmetric) mass 56 signal in the LURE data set, modeled using eq 6 with τ_d and τ as given in the Experimental Section. The five reliable points obtained with $\tau_d = 0.20$ μs allowed the assignment of the TS energy barrier and imaginary frequency with improved accuracy. Points for higher τ_d values come from Figure 3.

it is produced by a metastable reaction. It is possible to measure the dissociation rate constant by modeling the increase in the sharp m/z 56 peak with delay time, a technique pioneered by Stockbauer, Parr, and Rosenstock, who measured a number of dissociation rates using this approach.[25−27] However, in the present work, we only use these data as an additional test of the derived rate constants, as will be discussed shortly.

Variable delay TOF spectra, such as shown in Figure 3, were collected at only one photon energy (10.00 eV). TOF spectra at other photon energies were obtained only with the minimum pulser delay of 0.20 μs. The results of these spectra are summarized in Figure 4 as a breakdown diagram in which the fractional abundance of the parent ion and the two daughter ions are displayed as a function of the photon energy. The $C_4H_8^+$ signal is comprised of both the sharp peak and the asymmetric portion. However, any $C_4H_8^+$ ions that were formed in the drift region (i.e., after 2.13 μs) have the same TOF as the parent ions and are thus included in the parent ion signal. The fraction of ions that decay after 2.13 μs (parent ions) decreases with the photon energy. Thus, the breakdown diagram provides another opportunity to extract the dissociation rate constant.

A final data set is obtained from the ratio of the sharp $C_4H_8^+$ peak to the area of the asymmetric peak as a function of the photon energy. This ratio is displayed in Figure 5 for an ion extraction pulse delay of 0.20 μs at all energies investigated as well as the ratio at several delay times at a photon energy of 10.00 eV (also shown in Figure 3). We thus have a total of three independent methods for determining the dissociation rate constant for the HBr loss reaction: the asymmetric TOF distribution obtained at UNC, the breakdown diagram obtained at LURE, and the ratio of the symmetric to the asymmetric HBr loss peak obtained at LURE.

Ab Initio Molecular Orbital Calculations

All of the calculations were performed using the Gaussian 94 program[28] installed on either a Convex C3840 at UNC or a Cray T916 at the North Carolina Supercomputer Center. Calculations were performed at several levels of theory up to the MP2/6-31g* level. Using this setup, we have obtained fully optimized neutral, molecular ion, ion−molecule complex, and the H transfer transition-state (TS) geometries. The TS was tested using the intrinsic reaction coordinate (IRC) method of Gaussian 94. Geometries for the ionic species are shown in Figure 6.

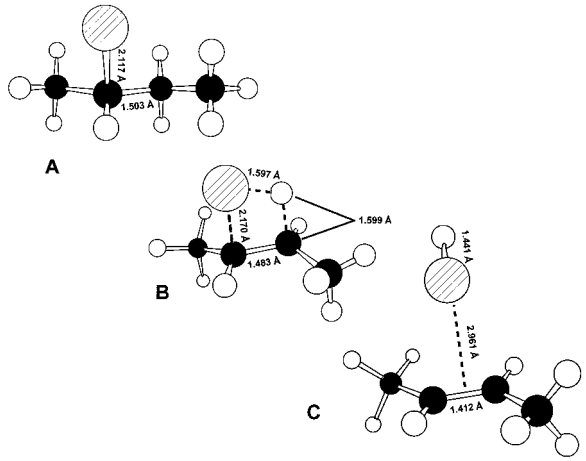

Figure 6. Calculated geometries of (A) molecular ion, (B) HBr loss transition state, and (C) ion−dipole complex. The geometries were optimized with ab initio MO calculations using the MP2/6-31G* basis set.

In the molecular ion (A), charge and spin are both localized at the Br atom. The C−Br length has increased from 1.984 Å in the neutral molecule to 2.117 Å in the ion. At the same time, the C_2-C_3 bond distance has decreased slightly from 1.521 to 1.503 Å.

The TS (Figure 6B) corresponds to a four-atom concerted process in which both the C_3-H and C_2-Br distances have increased from 1.095 to 1.599 Å and from 2.117 to 2.171 Å, respectively. On the other hand, the C_2-C_3 and Br−H bond lengths have decreased from 1.503 to 1.483 Å and from 3.121 to 1.597 Å, respectively. Thus, the hydrogen atom is equidistant from C_3 and Br. The charge is located on the hydrogen atoms (mostly on the one being transferred), and spin is at C_3.

The ion−dipole complex (Figure 6C) is an intermediate structure along the way to HBr loss products. The charge and spin are both shared between C_2 and C_3 atoms. This bond is a partial double bond, with a length of 1.412 Å. The Br−H bond length is now quite short (1.441 Å) with the Br lying 2.961 Å above the C_2-C_3 bond and the H pointed a little away from the carbon ion group. In this ion−dipole complex the remaining bond distances are nearly what they are in the isolated molecule and ion.

TABLE 1: Vibrational Frequencies Used in Boltzmann and RRKM Calculations[a]

species	vibrational frequencies/cm^{-1}
neutral 2-bromobutane (h-9)	81, 167, 196, 235, 344, 524, 626, 780, 800, 892, 974, 1011, 1022, 1061, 1091, 1165, 1219, 1276, 1293, 1360, 1386, 1399, 1452, 1465, 1471, 1873, 2019, 2899, 2926, 2974, 2997, 3012, 3030, 3137, 3379, 3514
neutral 2-bromobutane (d-9)	92, 169, 174, 187, 249, 297, 385, 472, 582, 683, 705, 753, 770, 869, 891, 960, 982, 1002, 1013, 1052, 1057, 1061, 1063, 1071, 1115, 1144, 1238, 2103, 2107, 2120, 2189, 2202, 2230, 2231, 2247, 2249
2-bromobutane molecular ion (h-9)	100, 157, 182, 231, 244, 289, 415, 427, 742, 807, 905, 963, 989, 1019, 1089, 1130, 1188, 1244, 1274, 1357, 1375, 1397, 1425, 1440, 1449, 1455, 1472, 2891, 2906, 2920, 2982, 2997, 3004, 3013, 3040, 3045
2-bromobutane molecular ion (d-9)	87, 130, 166, 169, 182, 250, 355, 374, 560, 666, 687, 725, 746, 854, 881, 930, 947, 986, 1008, 1029, 1038, 1040, 1059, 1062, 1100, 1134, 1230, 2088, 2099, 2119, 2208, 2214, 2221, 2222, 2253, 2260
TS connecting molecular ion and ion−molecule complex (h-9)	94, 170, 201, 244, 262, 321, 400, 448, 615, 793, 816, 924, 977, 991, 1033, 1074, 1122, 1157, 1271, 1374, 1378, 1391, 1433, 1439, 1447, 1452, 1509, 2902, 2918, 2990, 3008, 3017, 3025, 3041, 3051, 1265i
TS connecting molecular ion and ion−molecule complex (d-9)	81, 125, 178, 182, 220, 282, 330, 393, 472, 585, 667, 701, 727, 772, 854, 868, 910, 992, 1007, 1027, 1030, 1034, 1038, 1088, 1101, 1148, 1288, 2090, 2101, 2208, 2224, 2227, 2231, 2255, 2264, 951i

[a] All frequencies are corrected by Pople's 0.9427 factor (ref 27); h-9 frequencies are given first and then d-9 frequencies.

TABLE 2: Electronic and Zero-Point Vibrational Energies of Relevant Species[a]

species	MP2 energy/ hartrees	h-9 ZPVE/ kJ mol^{-1}	h-9 relative energy/eV	d-9 ZPVE/ kJ mol^{-1}	d-9 relative energy/eV
2-bromobutane neutral	−2727.253 598 1	336.86	−9.592	217.02	−9.777
2-bromobutane molecular ion	−2726.892 994 6	315.56	0	213.56	0
sec-$C_4H_9^+$	−156.917 139 7	303.49		205.56	
Br atom	−2569.955 833 3				
total Br loss products	−2726.872 973 0	303.49	0.5448	205.56	0.5870
TS (HBr)	−2726.856 088 8	295.52	0.7965	200.55	0.8694
ion−molecule complex	−2726.898 971 4	295.40	−0.3716	200.55	−0.2975
Br loss products (present experiment)			0.327		0.369(2)[b]
HBr loss products (literature)[19,28,29]			−0.1588		

[a] ZVPE is zero-point vibrational energy obtained using Pople's 0.9646 correction factor (ref 27). [b] This value is calculated from the experimental h-9 value and the ab initio ZPVE difference.

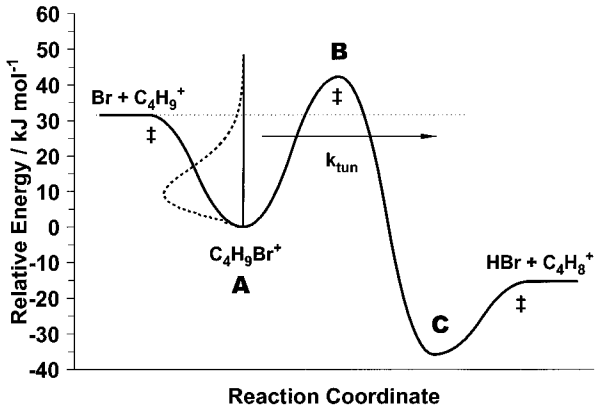

Figure 7. Potential energy diagram for the dissociation of 2-bromobutane ions. The thermal distribution of internal energies at 298 K is plotted on the graph to show that there is always a significant population of ions above the Br loss threshold. Below this energy, ions can tunnel through the HBr loss barrier. The energy of the ion−dipole complex formed between HBr and $C_4H_8^+$ was obtained from ab initio calculations.

The vibrational frequencies given in Table 1 have been corrected by a constant factor as suggested by Pople et al.[29] Frequencies are also given for the fully deuterated species. The relevant energies for these ionic structures are tabulated in Table 2, along with zero-point vibrational energies which were used to determine the relative energies of bromobutane, the molecular ion, transition state, and the ion−dipole complex. The results are also shown as a potential energy diagram in Figure 7. As a measure of the reliability of these calculations, we note that the ionization energy is calculated to be 9.59 eV compared to the experimental value of 9.98 eV. The Br loss channel is calculated to lie 0.545 eV above the ionization energy, while the experimental value was found to be 0.327 eV. Although the ionization energy prediction is not expected to be excellent, both of these differences may be attributable to a ∼35 kJ mol^{-1} underestimation of the molecular ion energy.

Although no data with fully deuterated samples were collected, we present in Tables 1 and 2 also the calculated results for the d-9 analogue. This will be used to make certain predictions concerning tunneling in fully deuterated 2-bromobutane ions.

Data Analysis and Discussion

The observation of "simultaneous" fast and slow production of product ions in energy-selected reactions requires some comment. Two-component decay of ions has been observed a number of times in recent years.[30,31] They can be explained in some cases by a competitive rapid dissociation and rapid isomerization to a lower energy structure followed by a slow dissociation from the lower energy isomer. This two-component behavior can be observed even when the ions are prepared with perfect energy resolution. In such systems, the ratio of fast to slow component varies quite gradually with energy and generally increases with energy because the fast reaction is often associated with a simple bond-breaking step while the rearrangement reaction involves a tight transition state. For a thermal distribution of reactant ions, however, a second possible source of two-component decay exists. If a reaction to the lowest energy product is slow, while the reaction rate to the higher

energy product is fast, the thermal distribution of ion internal energies can be divided into two classes: those with energy less than the second dissociation limit, which dissociate exclusively to the first product with a slow rate constant, and those ions with energy in excess of the second dissociation limit, which dissociate exclusively to the second product ion with a fast rate constant. Thus, there is never a real competition between the two reaction channels. If these ions could be prepared with perfect energy resolution, one would observe only one reaction occurring for a given ion internal energy.

To explain the occurrence of a reaction that proceeds slowly despite a low apparent activation energy, however, requires some explanation. Normally reactions occur more rapidly for lower energy transition states. One exception is when the reaction path of interest competes with production of lower energy structure. However, another possible explanation is that the classical transition-state energy is in fact higher, with reaction proceeding at low energy by tunneling through the TS barrier.

For a number of reasons, we conclude that the two-component behavior in the dissociation of 2-bromobutane ions is a result of the competitionless mechanism in which the slow reaction involves tunneling. A similar model was proposed by Heinrich et al. for the case of CH_3/CH_4 loss from acetone ions.[5] The model potential energy diagram for the 2-bromobutane ion system is illustrated in Figure 7. In this model, the HBr loss reaction is slow because it proceeds via tunneling through the H atom transfer barrier. Once the energy of the ion is in excess of the Br loss onset, the dissociation yields exclusively the $C_4H_9^+$ ion product. This explains why no HBr loss product is observed above the Br loss threshold, and the rapid change in the fast-to-slow ratio rules out the possibility of isomerization and dissociation in competition being responsible for the observed apparent two-component dissociation behavior. In further support of the tunneling mechanism, we note that reaction in the absence of tunneling would yield a rate that is much faster than measured. Using the standard RRKM rate constant equation[9]

$$k_{\mathrm{RRKM}}(\epsilon) = \frac{\sigma N^{\ddagger}(\epsilon - E_0)}{h\rho(\epsilon)} \qquad (1)$$

with vibrational frequencies determined from ab initio MO calculations, we calculate that the minimum dissociation rate constant for Br loss is in excess of 10^9 s^{-1}. In this expression, $N^{\ddagger}$ is the sum of internal energy states between 0 and $\epsilon - E_0$, $\rho(\epsilon)$ is the density of states at energy ϵ, and σ is the ratio of symmetry numbers for reactant and the transition state. Because both 2-bromobutane and the transition state have no symmetry, σ is 1. The rate for HBr loss would be even faster if the barrier for HBr loss were below that of Br loss. Thus, in the following sections, we analyze the results in terms of the model proposed in Figure 7.

The Br Loss Onset. Before analyzing the full breakdown diagram, it is helpful to determine the 0 K onset for the Br loss reaction. By combining the $C_4H_8^+$ signal with the parent ion, a modified breakdown diagram can be constructed for the Br loss product, $C_4H_9^+$. Such a breakdown diagram for the LURE data set, shown in Figure 8, can be analyzed without regard to the slow dissociation rate for HBr loss. That is, we assume that all ions below the Br loss onset are either parent ions or HBr loss ions and that all ions produced above the Br loss onset are exclusively $C_4H_9^+$ ions. The only two parameters needed are the distribution of internal energies of the bromobutane ions and the Br loss dissociation limit. The Boltzmann distribution

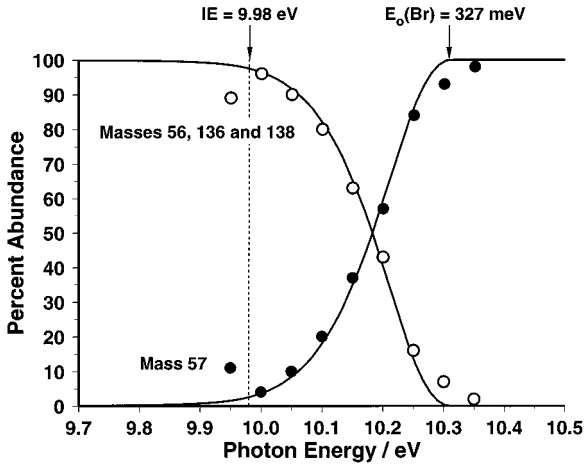

Figure 8. A modified breakdown diagram obtained by combining the parent and $C_4H_8^+$ ion signals in Figure 4. This curve is used to measure the Br loss threshold by assuming that ions with an internal energy in excess of the Br loss threshold yield exclusively this product. The solid line is a fitted breakdown diagram using the 298 K internal energy distribution and varying the Br loss onset for best fit.

of internal energies is given by

$$P(E) = \frac{\rho(E)\mathrm{e}^{-E/RT}}{\int_0^{\infty} \rho(E)\mathrm{e}^{-E/RT}\,\mathrm{d}E} \qquad (2)$$

where $\rho(E)$ is the density of states that is calculated with the vibrational frequencies for the neutral bromobutane molecule obtained from ab initio MO calculations. In other words, it is assumed that the neutral distribution of internal energies is transferred to the ion upon photoionization. The solid lines through the data points in Figure 8 are the result of using a 298 K thermal energy distribution (including rotations and vibrations) and an assumed dissociation limit of 10.307 eV. From the quality of this fit we conclude that our neat beam of bromobutane has an internal temperature of 298 K. Had our sample experienced real molecular beam cooling, the breakdown diagram would have shown a much sharper crossover at a higher photon energy, closer to the 0 K threshold. It is evident that the 298 K crossover energy is shifted to lower energy by the mean thermal energy of 138 meV. This analysis leads to a new 0 K heat of formation of the *sec*-butyl cation of 794 ± 3 kJ mol^{-1}, which is 7.2 kJ mol^{-1} lower than the value listed by Lias et al.[32,33]

Fitting of the Full Breakdown Diagram. With a good value for the Br loss threshold, it is possible to fit the full breakdown diagram including the HBr loss reaction whose contribution is modeled using the statistical rate theory. According to the model shown in Figure 7, the HBr loss channel contributes only in a small energy range. The lower energy cutoff is "soft" and is determined by the rate of dissociation which must be sufficiently fast to form products in less than 2.13 μs. On the high-energy side, any ions with internal energy greater than 0.327 eV will produce exclusively Br loss products. Thus, we model the mass 56 signal in the breakdown curve using the population-weighted calculated rate constant function of ion internal energy, $k(\epsilon)$:

$$S_{56}(h\nu) = \int_{h\nu\text{-IE}}^{E_0(\mathrm{Br})} P(\epsilon + \mathrm{IE} - h\nu)(1 - \mathrm{e}^{-k(\epsilon)\tau})\,\mathrm{d}\epsilon \qquad (3)$$

in which the $1 - \exp(-k(\epsilon)\tau)$ term represents the m/z 56 products for ions with internal energy ϵ formed within $\tau = 2.13$

μs. The Br loss *m*/*z* 57 signal, as just discussed, is given by

$$S_{57}(h\nu) = \int_{E_0(\mathrm{Br})}^{\infty} P(\epsilon + \mathrm{IE} - h\nu)\, \mathrm{d}\epsilon \qquad (4)$$

Finally, the parent ion is given simply by $S_{\mathrm{parent}} = 1 - S_{56} - S_{57}$.

Since we know that the thermal population is one corresponding to 298 K and we know the Br loss onset, the only adjustable parameter for fitting the full breakdown diagram is the $k(\epsilon)$ function. Any convenient mathematical function could be used to model this $k(\epsilon)$ curve. However, we chose to utilize a $k(\epsilon)$ curve using RRKM theory, modified by including the effect of tunneling. Two parameters, the barrier height and the imaginary frequency associated with the curvature at the top of an Eckart barrier, were used as adjustable parameters.

As suggested by Miller,[8,9] the RRKM rate constant modified to include the effect of tunneling is given by

$$k_{\mathrm{RRKM}}(\epsilon) = \frac{\sigma}{h\rho(\epsilon)} \int_{-E_0}^{\epsilon - E_0} \kappa_{\mathrm{tun}}(\xi)\, \rho^{\ddagger}(\epsilon - E_0 - \xi)\, \mathrm{d}\xi \qquad (5)$$

where we are now explicitly integrating the TS density of states $\rho^{\ddagger}$ multiplied by the tunneling probability κ_{tun} to obtain an effective TS sum of states $N^{\ddagger}$ for the tunneling reaction. In the integration, ξ is the energy in the reaction coordinate as measured from the top of the TS barrier and is less than zero below the barrier where only tunneling can occur and greater than zero above the barrier. This definition is convenient because the same $k(\epsilon)$ function can be used to evaluate the rate constant below and above the barrier. The ion internal energy ϵ retains the same meaning as in eqs 1 and 3. This total ion energy is partitioned between energy in the one-dimensional reaction coordinate ($\epsilon - E_o - \xi$) and all the other internal degrees of freedom of the ion ($E_0 + \xi$). The integration is over all combinations of energy in the reaction coordinate and in the transition-state degrees of freedom.

The tunneling probability function is obtained from the Eckart barrier.[9,34] This function depends only upon the reaction energy ΔE, activation energy E_0, and imaginary frequency $\nu^{\ddagger}$ of the reaction coordinate normal mode. The values for ΔE, E_0, and $\nu^{\ddagger}$ were obtained from the ab initio MO calculations (see Tables 1 and 2). However, because the calculated dissociation rate constants depend very sensitively on the value of E_0 and $\nu^{\ddagger}$, only the ΔE value was taken without adjustment from the ab initio MO calculations. Figure 7 shows a potential well on the product side which is associated with the ion−dipole well between the HBr and $C_4H_8^+$ products. The ΔE value for the Eckart barrier was thus taken to be −0.372 eV (−36.85 kJ/mol). In addition, the real vibrational frequencies for the molecular ion and the transition state were taken without adjustment from the ab initio MO results shown in Table 1. These were used for calculating sums and densities of states. Thus, E_0 and $\nu^{\ddagger}$ were used as the only adjustable parameters in fitting the breakdown diagram.

The resulting best fit is shown as the solid line through the data points in Figure 4. Since we can adjust both the activation energy and the magnitude of the imaginary frequency, we used the ratio R of sharp to broad mass 56 TOF signal at a delay time of 0.2 μs in Figure 5 to help minimize the uncertainty in the determination. This ratio is given by

$$R = \frac{\text{sharp mass 56 peak area}}{\text{asymmetric mass 56 peak area}} = \frac{\int_{h\nu-\mathrm{IE}}^{E_0(\mathrm{Br})} P(\epsilon - \mathrm{IE} - h\nu)(1 - e^{-k(\epsilon)(\tau_e+\tau_d)})\, \mathrm{d}\epsilon}{\int_{h\nu-\mathrm{IE}}^{E_0(\mathrm{Br})} P(\epsilon - \mathrm{IE} - h\nu)(e^{-k(\epsilon)(\tau_e+\tau_d)} - e^{-k(\epsilon)(\tau)})\, \mathrm{d}\epsilon} \qquad (6)$$

in which $(\tau_e + \tau_d)$ is the time required to apply the ion extraction pulse, while τ is the total time the parent ion spends in the first acceleration region. We found the best fit to both experimental results with an activation barrier of 0.438 ± 0.007 eV (as shown in Figure 7) and $\nu^{\ddagger}$ = 1245 ± 10 cm^{-1}. The derived microcanonical rate constant function of ion internal energy is shown in Figure 9. As a test of the derived rate constants in Figure 9, we modeled the asymmetric $C_4H_8^+$ TOF distributions such as that shown in Figure 2 which were obtained at UNC. The $k(\epsilon)$ curve in Figure 9 was used to generate effective rate constants for the 230 K distribution (with the hot electron tail) which were fit to the observed rate constant data points, also shown in that figure.

It is interesting that, relative to the derived rate constant function that fits the bulk of the data (the UNC data in Figure 2, the LURE breakdown data in Figure 4, and the R value in Figure 5 at an extraction delay of 0.2 μs), the experimental R values for the longer delays of 1.20 and 2.12 μs were found to be 11% and 19% too low. We attribute this to loss of translationally energetic fragment ions from the ionization region prior to extraction. The dissociation reaction apparently produces translationally energetic products that can escape the ionization region before the extraction pulse is finally applied. Since the asymmetric signal results from ions that dissociate quite late, the fact that they spend most of their time as parent ions helps to ensure that they are detected. Thus, as the delay time is increased, more and more of the early reaction products are lost.

Because the tunneling probability k_{tun} depends very sensitively on the ion energy, the resulting rate varies by 1.5 orders of magnitude over the 80 meV average thermal energy in the UNC molecular beam data. For this reason, the observed HBr loss signal, which is proportional to the rate constant, results from only a very narrow ion internal energy range near the Br loss threshold. Thus, the effective rate constant varies only slightly over the energy range investigated. The inclusion of the hot electron tail in the electron energy resolution function of the UNC apparatus results in observed HBr loss data above the Br loss onset. The experimental and predicted effective rate constants agree extremely well over the whole energy range investigated.

Will Perdeuterio-2-bromobutane Ions Decay by Tunneling?

We can use the results from this experiment to predict the behavior of perdeuterio-2-bromobutane. The frequencies calculated for this isotopomer were used in the RRKM calculation, and the neutral d-9 frequencies were used to obtain a thermal energy distribution. Changes in zero-point vibrational energy shift the classical barrier heights from 0.327 to 0.369 eV for Br loss and from 0.438 to 0.511 eV for DBr loss. The imaginary frequency was taken to be the same percentage of the ab initio MO result as obtained for h-9. That is, 1265:1245 = 951:936.

The results of this calculation show that we can expect to see no DBr loss product in a d-9 experiment. At any given ion internal energy ϵ, d-9 tunneling RRKM rate constants are lower than for h-9 by at least 3 orders of magnitude. As a result, the

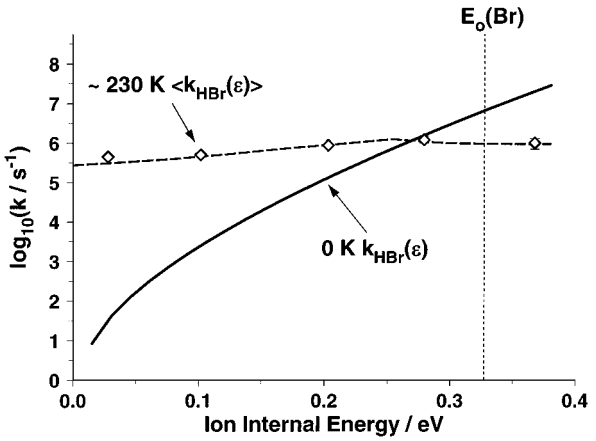

Figure 9. Microcanonical rate constants measured from experiments at UNC and at LURE by fitting to a calculation using $E_0(\mathrm{HBr}) = 0.438$ eV and $\nu^{\ddagger} = 1245$ cm^{-1}. This function rises much more sharply than do similar known rearrangement reactions that do not involve tunneling. The dashed line running through the UNC "effective" rate constant data is obtained from this calculation using an ion internal energy distribution that includes a 230 K vibrational Boltzmann distribution and a hot electron tailing function. Effective rate constants above the Br loss onset result from this hot electron tail.

minimum rate constant for observation of HBr signal ($\sim 10^4$ s^{-1}) moves to above the Br onset, so that no significant DBr loss signal can be expected. We predict the DBr signal to remain below 0.5% of total ions. The Br loss crossover point for a thermal sample is expected to remain at nearly the same ion energy (C_0 − IE) because the zero-point energy difference offsets the thermal energy shift.

Conclusion

The HBr loss reaction of 2-bromobutane ions is explained in terms of quantum-mechanical tunneling through a proton-transfer activation barrier. Ab initio MO calculations provide vibrational frequencies for RRKM rate constant evaluation in good agreement with experiment. Ab initio transition-state energies obtained at the MP2/6-31g* level of theory, however, are not reliable and in this case were high by ~35 kJ mol^{-1}. This is quite similar to the ~32 kJ mol^{-1} overestimation observed by Booze et al.[4] in the case of ethyl chloride ions. It is hoped that careful studies such as these of transition states through which tunneling may occur will help with future application of rate constant calculations and interpretation of ab initio molecular orbital results.

In addition, we have obtained new accurate measurements of 2-bromobutane adiabatic ionization energy (9.98 ± 0.02 eV) and Br loss appearance energy (10.307 ± 0.02 eV). This has allowed the derivation of 0 K heats of formation for 2-bromobutane cation (880.1 ± 2.7 kJ mol^{-1}) and the *sec*-butyl cation (794 ± 3 kJ mol^{-1}).

Acknowledgment. We thank Michel Vervloet, who is in charge of the SAPHIRS experimental setup at LURE, for his kind help with the experiment, as well as Martine Richard-Viard, who coordinated its construction. The LURE staff is acknowledged for operating the Super-ACO storage ring and general facilities. In addition, we are grateful for grants from the U.S. Department of Energy and the North Carolina Supercomputer Center.

References and Notes

(1) Polik, W. F.; Moore, C. B.; Miller, W. H. *J. Chem. Phys.* **1988**, *89*, 3584.
(2) Polik, W. F.; Guyer, D. R.; Miller, W. H.; Moore, C. B. *J. Chem. Phys.* **1990**, *92*, 3471.
(3) Morrow, J. C.; Baer, T. *J. Phys. Chem.* **1988**, *92*, 6567.
(4) Booze, J. A.; Weitzel, K. M.; Baer, T. *J. Chem. Phys.* **1991**, *94*, 3649.
(5) Heinrich, N.; Luage, F.; Lifshitz, C.; Schwarz, H. *J. Am. Chem. Soc.* **1988**, *110*, 8183.
(6) Hristendahl, G.; Uggerud, E. *Org. Mass Spectrom.* **1991**, *26*, 67.
(7) Heinrich, N.; Drewello, T.; Burgers, P. C.; Morrow, J. C.; Schmidt, J.; Kulik, W.; Terlouw, J. K.; Schwarz, H. *J. Am. Chem. Soc.* **1992**, *114*, 3776.
(8) Miller, W. H. *J. Am. Chem. Soc.* **1979**, *101*, 6810.
(9) Baer, T.; Hase, W. L. *Unimolecular Reaction Dynamics: Theory and Experiments*; Oxford: New York, 1996.
(10) Schroder, D.; Sulzle, D.; Dutuit, O.; Baer, T.; Schwarz, H. *J. Am. Chem. Soc.* **1994**, *116*, 6395.
(11) Oliveira, M. C.; Baer, T.; Olesik, S.; Almoster Ferreira, M. A. *Int. J. Mass Spectrom. Ion Processes* **1988**, *82*, 299.
(12) Traeger, J. C. *Org. Mass Spectrom.* **1981**, *16*, 193.
(13) Rosenstock, H. M.; Buff, R.; Ferreira, M. A. A.; Lias, S. G.; Parr, A. C.; Stockbauer, R.; Holmes, J. L. *J. Am. Chem. Soc.* **1982**, *104*, 2337.
(14) Almoster Ferreira, M. A.; Costa Cabral, B. J.; Oliveira, M. C.; Baer, T. *Org. Mass Spectrom.* **1993**, *28*, 1229.
(15) Miller, B. E.; Baer, T. *Chem. Phys.* **1984**, *85*, 39.
(16) Traeger, J. C. *Int. J. Mass Spectrom. Ion Phys.* **1980**, *32*, 309.
(17) Baer, T.; Booze, J. A.; Weitzel, K. M. In *Vacuum Ultraviolet Photoionization and Photodissociation of Molecules and Clusters*; Ng, C. Y., Ed.; World Scientific: Singapore, 1991; p 259.
(18) Weitzel, K. M.; Booze, J. A.; Baer, T. *Chem. Phys.* **1991**, *150*, 263.
(19) Baer, T.; Dutuit, O.; Mestdagh, H.; Rolando, C. *J. Phys. Chem.* **1988**, *92*, 5674.
(20) Richard-Viard, M.; Delboulbe, A.; Vervloet, M. *Chem. Phys.* **1996**, *209*, 159.
(21) Hashmall, J.; Heilbronner, E. *Angew. Chem., Int. Ed. Engl.* **1970**, *9*, 305.
(22) Pedley, J. B.; Naylor, R. D.; Kirby, S. P. *Thermochemical Data of Organic Compounds*; Chapman and Hall: London, 1986.
(23) Wagman, D. D.; Evans, W. H. E.; Parker, V. B.; Schum, R. H.; Halow, I.; Mailey, S. M.; Churney, K. L.; Nuttall, R. L. *The NBS Tables of Chemical Thermodynamic Properties, J. Phys. Chem. Ref. Data, Vol. 11, Suppl. 2*; NSRDS: U.S. Government Printing Office: Washington, DC, 1982.
(24) Keister, J. W.; Baer, T.; Evans, M.; Ng, C. Y.; Hsu, C. W. *J. Phys. Chem. A* **1997**, *101*, 1866.
(25) Rosenstock, H. M.; Stockbauer, R.; Parr, A. C. *J. Chim. Phys.* **1980**, *77*, 745.
(26) Rosenstock, H. M.; Stockbauer, R.; Parr, A. C. *Int. J. Mass Spectrom. Ion Processes* **1981**, *38*, 323.
(27) Dannacher, J.; Rosenstock, H. M.; Buff, R.; Parr, A. C.; Stockbauer, R.; Bombach, R.; Staddelmann, J. P. *Chem. Phys.* **1983**, *75*, 23.
(28) Frisch, M. J.; Trucks, G. W.; Schlegel, H. B.; Gill, P. M. W.; Johnson, B. G.; Robb, M. A.; Cheeseman, J. R.; Keith, T. A.; Petersson, G. A.; Montgomery, J. A.; Raghavachari, K.; Al-Laham, M. A.; Zakrzewski, V. G.; Ortiz, J. V.; Foresman, J. B.; Cioslowski, J.; Stefanov, B. B.; Nanayakkara, A.; Challacombe, M.; Peng, C. Y.; Ayala, P. Y.; Chen, W.; Wong, M. W.; Andres, J. L.; Replogle, E. S.; Gomperts, R.; Martin, R. L.; Fox, D. J.; Binkley, J. S.; Defrees, D. J.; Baker, J.; Stewart, J. P.; Head-Gordon, M.; Gonzalez, C.; Pople, J. A. *GAUSSIAN 94*, Revision C.3; Gaussian Inc.: Pittsburgh, PA, 1995.
(29) Pople, J. A.; Scott, A. P.; Wong, M. W.; Radom, L. *Isr. J. Chem.* **1993**, *33*, 345.
(30) Duffy, L. M.; Keister, J. W.; Baer, T. *J. Phys. Chem.* **1995**, *99*, 17862.
(31) Baer, T.; Mazyar, O. A.; Keister, J. W.; Mayer, P. M. *Ber. Bunsen-Ges. Phys. Chem.* **1997**, *101*, 478.
(32) Lias, S. G.; Bartmess, J. E.; Liebman, J. F.; Holmes, J. L.; Levin, R. D.; Mallard, W. G. *Gas-Phase Ion and Neutral Thermochemistry, J. Phys. Chem. Ref. Data, Vol 17, Suppl. 1*; NSRDS; U.S. Government Printing Office: Washington, DC, 1988.
(33) Lias, S. G.; Liebman, J. F.; Levin, R. D.; Kafafi, S. A.; Stein, S. E. *Postive Ion Energetics, Version 2 NIST Standard Reference Database 19A*; NIST: Gaithersburg, MD, 1993.
(34) Eckart, C. *Phys. Rev.* **1930**, *35*, 1303.